DIRECT DISPLACEMENT-BASED DESIGN OF A RC WALL-STEEL EBF DUAL SYSTEM WITH ADDED DAMPERS

Timothy J. Sullivan[1]

SUMMARY

An innovative application of Direct Displacement-Based Design (DBD) is presented for a modern 8-storey dual system structure consisting of interior concrete walls in parallel to a number of large steel eccentrically braced frames, fitted with visco-elastic dampers at link positions. The innovative DBD methodology lets the designer directly control the forces in the structure by choosing strength proportions at the start of the design procedure. The strength proportions are used to establish the displaced shape at peak response and thereby establish the equivalent single-degree-of-freedom system design displacement, mass and effective height. A new simplified formulation for the equivalent viscous damping of systems possessing viscous dampers is proposed which also utilises the strength proportions chosen by the designer at the start of the process. The DBD approach developed is relatively quick to use, enabling the seismic design of the 8-storey case study structure to be undertaken without the development of a computer model. To verify the ability of the design method, non-linear time-history analyses are undertaken using a suite of spectrum-compatible accelerograms. These analyses demonstrate that the design solution successfully achieves the design objectives to limit building deformations, and therefore damage.

INTRODUCTION

Direct Displacement-Based Design (DBD) [1] has now been developed to a point that engineers can start to take advantage of it in practice. Not only does Direct DBD overcome the fundamental drawbacks of force-based design, but the methodology also offers designers a rational means of designing structural systems that may not be classified within a traditional design code approach. In this paper, the concept design of a modern 8-storey commercial building is undertaken using Direct DBD. The building, shown in Figure 1 and Figure 2, is an 8-storey dual system structure consisting of interior concrete walls in parallel to a number of large steel eccentrically braced frames. In order to minimise residual deformations of the structure, a traditional EBF system is not utilised and instead the EBF links incorporate centrally located visco-elastic dampers. The position of these dampers is indicated in Figure 2. The direction of earthquake excitation considered in this work is also indicated in Figure 2.

The rather unusual combination of structural elements proposed for this building was driven by a combination of factors, as is rather common in practice. The concrete walls and floors offer good acoustic performance and fire resistance. The steel gravity framing offers speed in erection and enables relatively slim floors, while the EBF system provides the building with peculiar aesthetic qualities and good lateral resistance. The internal steel framing resists gravity loads only (ensured by appropriate detailing) and the 200 mm thick RC floors are assumed to provide rigid diaphragm action in-plane. In order to avoid cluttering Figure 2, details of the internal gravity load resisting system are not shown but column positions and beam lines are indicated.

The concept design solution for the building is developed for the damage-control limit state and a non-structural drift limit of 2.0%. The seismicity of the site for an event with 10% probability in 50 years is represented with the UBC97 [2] spectrum for soil type C at a PGA of 0.4g.

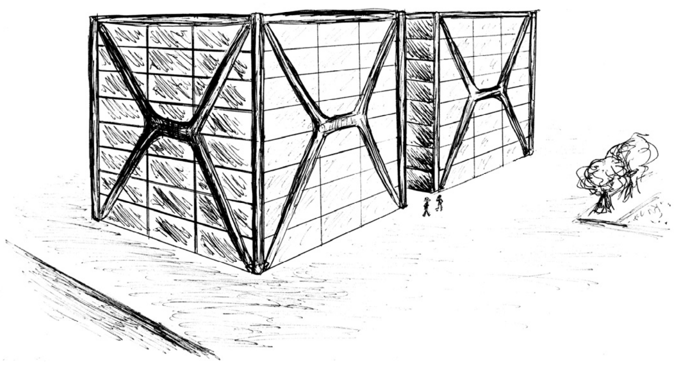

Figure 1: ***Sketch of the 8-storey case-study building.***

[1] *Assistant Professor, University of Pavia, Italy (Member)*

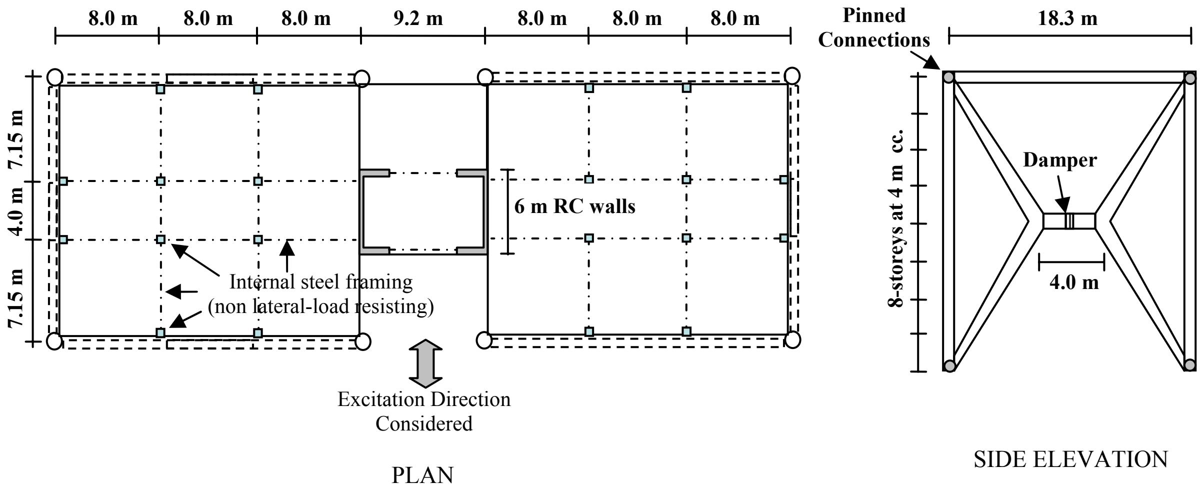

Figure 2: ***Plan and Elevation of the 8-storey dual-system case-study building (not to scale).***

DIRECT DISPLACEMENT-BASED DESIGN

A method for the Direct DBD of Frame-Wall dual systems has been developed and tested by Sullivan *et al.* [3] and a methodology for the Direct DBD of systems with added damping has been proposed by Christopoulos and Filiatrault [4]. However, to the author's knowledge, a Direct DBD procedure has not previously been developed for the combination of structural systems incorporated in the case-study building. Furthermore, the methodology for systems with added damping [4] is iterative and therefore not very practical. As will be shown in this paper, the Direct DBD methodology developed for frame-wall dual systems by Sullivan *et al.* [3] can be relatively easily adapted to the case study structure, and the added damping devices can be accounted for without iteration.

General Procedure

The basic process of the Direct DBD procedure developed principally by Priestley *et al.* [1] is illustrated for a dual system in Figure 3. The first two steps in the procedure, shown as Fig. 3(a) and Fig. 3(b), aim to establish the effective mass, (m_e), height (h_e) and design displacement (Δ_d) of an equivalent SDOF system representation of the MDOF building, responding to a selected deformation limit (associated with either material strain or non-structural storey drift limits). This is based on the Substitute Structure approach pioneered by Gulkan and Sozen [5] and Shibata and Sozen [6].

As indicated in Figure 3(c), the ductility demand expected at the design deformation limit is then used to set an equivalent viscous damping value for the equivalent SDOF system. This equivalent viscous damping represents the energy dissipated by the structure and therefore the damping values vary depending on the hysteretic properties of the structural system being designed.

To account for the impact that energy dissipation has on the dynamic response, the design displacement-spectrum is then developed at the expected equivalent viscous damping level. As shown in Figure 3(d), the design displacement is then used to enter the highly-damped spectrum and read off the effective period that will ensure the design displacement is not exceeded. The effective period, T_e, can be related to an equivalent SDOF effective stiffness, K_{eff}, using Equation 1.

$$K_{eff} = 4\pi^2 \frac{m_e}{T_e^2} \tag{1}$$

where m_e is the effective mass of the equivalent SDOF system (established in steps a & b of the design procedure). Finally, the design base-shear, V_b, is obtained by multiplying the required effective stiffness by the design displacement, as shown in Equation 2.

$$V_b = K_{eff} \Delta_d \tag{2}$$

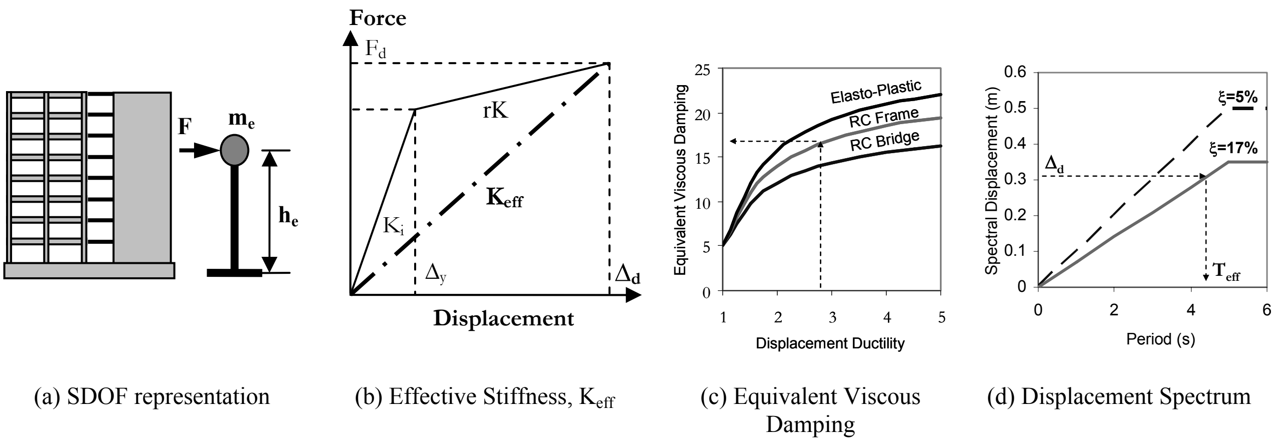

(a) SDOF representation (b) Effective Stiffness, K_{eff} (c) Equivalent Viscous Damping (d) Displacement Spectrum

Figure 3: ***Fundamentals of Direct Displacement-Based Design (adapted from [3]).***

As such, the design procedure is relatively simple. The challenge for dual-system case-study structures is to establish the appropriate equivalent viscous damping and the equivalent SDOF system values of effective mass, height and design displacement. As will be seen in the next section, these equivalent SDOF parameters can be established with knowledge of the design displacement profile expected for the building at the design deformation limit.

By considering the results of shake table tests on RC frame-wall systems, Sullivan *et al.* [7] found that the displacement profile of RC frame-wall systems is dependent on the curvature profile in the RC walls, which in turn is a function of the proportions of strength assigned to the walls and frames. Based on this observation, the design methodology presented in Figure 4 was developed by Sullivan *et al.* [3] for dual systems possessing RC walls and frames. This methodology will be extended here for the case-study building being examined.

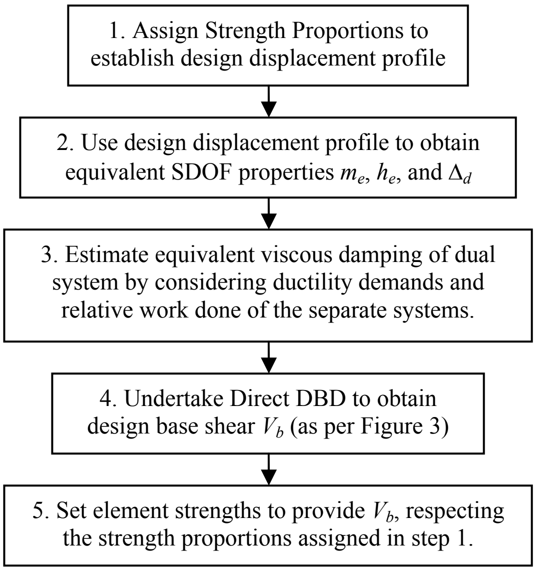

Figure 4: ***Design methodology for RC frame-wall systems [3] and extended here for the case-study building.***

Design Displacement Profile for the Dual System

As indicated in Figure 4, strength proportions are assigned at the start of the design procedure to give the design displacement profile. This is done by using the strength proportions to establish the moment profile and subsequently the curvature profile in the RC walls at peak response. Integration of the curvature profile then provides the displacement profile. Sullivan *et al.* [7] found that the displacement profile in RC frame-wall systems is well represented by summing the elastic displacement profile of the walls together with a linearly increasing displacement profile associated with inelastic rotation of a base plastic hinge in the RC walls, as shown by Equation 3.

$$\Delta_i = \Delta_{iy} + \left(\theta_d - \frac{\phi_{yWall} h_{cf}}{2}\right).h_i \tag{3}$$

where Δ_i is the design displacement for level i
θ_d is the design storey drift limit
ϕ_{yWall} is the wall yield curvature (Equation 5)
h_i is the height to level i
h_{cf} is the contra-flexure height in the walls
and Δ_{iy} is, given by Equation 4.

$$\Delta_{iy} = \frac{\phi_{yWall} h_{cf} h_i}{2} - \frac{\phi_{yWall} h_{cf}^2}{6} \qquad \text{for } h_i > h_{cf} \tag{4a}$$

$$\Delta_{iy} = \frac{\phi_{yWall} h_i^2}{2} - \frac{\phi_{yWall} h_i^3}{6h_{cf}} \qquad \text{for } h_i \le h_{cf} \tag{4b}$$

The contraflexure height in the walls, h_{cf}, can be obtained with knowledge of the strength proportions, as explained in subsequent paragraphs.

The yield curvature for U-shaped walls bending in the axis of the web can be approximated with reasonable accuracy [8] using only the longitudinal reinforcement yield strain and the wall length, as shown by Equation 5 [9]. Yield curvature expressions for other section shapes are available in [1].

$$\phi_{yWall} = 1.4\varepsilon_y / L_w \tag{5}$$

The yield displacement profile given by Equation 4 assumes a linear variation in wall curvature from the yield curvature at the base to zero at the contra-flexure height. As argued by Priestley and Paulay [10] this approach approximately accounts for tension shift and higher mode effects and as shown by Sullivan *et al.* [7] it appears to work relatively well for RC frame-wall systems.

For the case study dual system examined here, the assumption that the curvatures in the walls will dictate the displacement profile of the building, is made considering that the stiffness of the large wall sections is considerably greater than that of the EBF columns. One might anticipate that the diagonals of the EBF system would render the EBF very stiff and that therefore, these should be considered in setting the displaced shape. However, the diagonals are not connected directly to each floor level and are instead only connected to the top and bottom of the EBF columns. As such, the deformed shape of the structure from the ground to roof level is dependent on the curvatures of the stiffest elements, which are the wall sections. The EBF system resistance is still expected to influence the displaced shape, but in a secondary fashion through changes to the moment and therefore curvature profile in the walls. Note that the results of non-linear time-history analyses presented later in this paper also support the validity of this displaced shape assumption. As such, Equations 4 and 5 can be used to estimate the building's displaced shape, provided that the strength proportions of the EBF relative to the RC walls are considered in establishing the wall contraflexure height.

Contraflexure develops in a wall when a parallel structural system causes the upper levels of the wall to be bent in an opposite sense relative to the lower levels. This occurs in frame-wall structures because the frames tend to restrain the upper levels of the walls. It should also be expected for the case study structure being considered if the EBF system restrains a large amount of the lateral load. Figure 5 illustrates how the shear forces and bending moments are expected to vary according to the proportion of resistance assigned to the walls and EBFs respectively. Two cases are shown in order to demonstrate that with a large portion of the overturning assigned to the EBF system, the walls are expected to undergo reverse bending over their upper levels, developing a point of contraflexure at a height, h_{cf}. The contraflexure height is expected to reduce as the proportion of resistance carried by the EBF system increases.

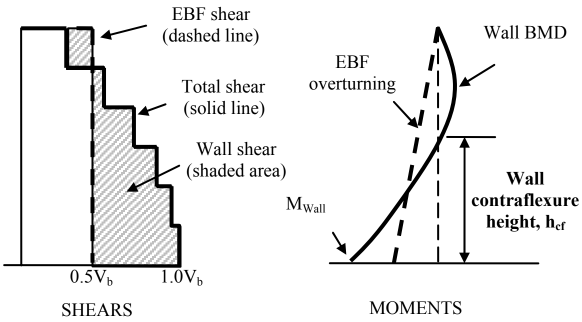

(a) High proportion of resistance assigned to EBF

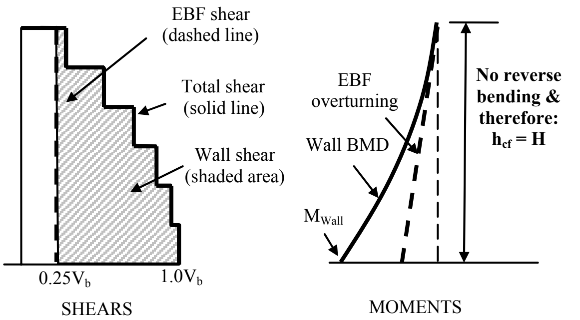

(b) Low proportion of resistance assigned to EBF

Figure 5: ***Affect of proportions of resistance on wall moment profile and contraflexure height.***

In order to determine the contraflexure height, the moment profile in the walls is required. This is calculated using the fundamental mode wall shear profile which is obtained using Equation 6 as the different between the total shear and the EBF shear proportions.

$$\frac{V_{i,wall}}{V_b} = \frac{V_{i,total}}{V_b} - \frac{V_{i,EBF}}{V_b} \tag{6}$$

where V_b is the total base shear, $V_{i,wall}$ is the wall shear at level i, $V_{i,total}$ is the total shear at level i, and $V_{i,EBF}$ is the EBF shear at level i.

For the purpose of establishing the inflection height, total fundamental mode inertia forces are assumed to act with a triangular distribution up the height of the structure. This approximation enables the total storey shear to be obtained as a function of the base shear as shown in Equation 7.

$$\frac{V_{i,total}}{V_b} = 1 - \frac{i\,(i-1)}{n\,(n+1)} \tag{7}$$

where n is the total number of storeys.

The proportion of the design shear resisted by the EBF is the choice of the designer. This is because the designer can control the forces that develop in the EBF when setting the characteristics of the visco-elastic dampers at the end of the design procedure and with knowledge of the required total base shear.

Considering the visco-elastic dampers at the centre of the EBF frames, one expects a velocity-dependent force component which is a function of the viscous characteristics of the damper in addition to a displacement-dependent force associated with the elastic characteristics of the device. In this work, the proportions of viscous and elastic damping forces were treated as design variables, such that the viscous damping force was set to be three times the elastic damping force. The proportion of overturning resisted by the EBF at peak response is set to 15% the total overturning demand (one could alternatively use shear proportions to simplify application of Equations 6 and 7). While this may at first appear low, it implies that the overturning resisted by the velocity-dependent component of the damped EBF system is therefore 45% the total overturning demand. Using these strength proportions, the internal shear distributions up the height of the structure are determined using Equations 6 and 7, as shown in Table 1, where the total inertia forces have been set to give a base shear of 100%. Note that the EBF is connected to the building at roof level and so provides a uniform shear resistance down the building height. The moments expected in the frame and wall systems are then found from the shear profiles and the resulting bending moment profiles are illustrated in Figure 6 as a proportion of the total overturning demand (currently an unknown).

As can be seen from Table 1 and Figure 6, because the frame resists a relatively low portion of the overturning at peak displacement response, the walls do not undergo reverse bending and therefore the contraflexure height corresponds to the total building height.

Substituting h_{cf} = 32 m into Equations 3 and 4, and evaluating the wall yield curvature (= 0.0057 m^{-1}) using Equation 5, the displacement profiles at wall yield and at the development of the design storey drift are obtained. These displacement profiles are reported on the right side of Table 1 and are illustrated in Figure 7.

Table 1: Internal force distribution and design displacement profiles.

		Internal Force Distribution for a Unit Base Shear, V_b					Displacement Profiles	
Level	**h_i (m)**	**$V_{i\ total}$**	**$V_{i\ frame}$**	**$V_{i\ Wall}$**	**$M_{i\ total}$**	**$M_{i\ Wall}$**	**$\Delta_{iy,wall}$ (Eq. 4)**	**Δ_i (Eq. 3)**
8	32				0.0	0.0	0.19	0.54
7	28	22%	10.6%	11.6%	0.9	0.5	0.16	0.46
6	24	42%	10.6%	31.0%	2.6	1.7	0.12	0.38
5	20	58%	10.6%	47.7%	4.9	3.6	0.09	0.31
4	16	72%	10.6%	61.6%	7.8	6.1	0.06	0.24
3	12	83%	10.6%	72.7%	11.1	9.0	0.04	0.17
2	8	92%	10.6%	81.0%	14.8	12.2	0.02	0.10
1	4	97%	10.6%	86.6%	18.7	15.7	0.00	0.05
0	0	100%	10.6%	89.4%	22.7	19.3	0.00	0.00

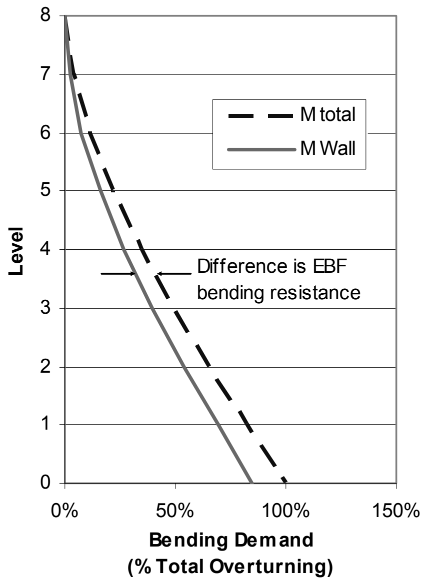

Figure 6: Bending moment profiles for the case-study building at the peak displacement response.

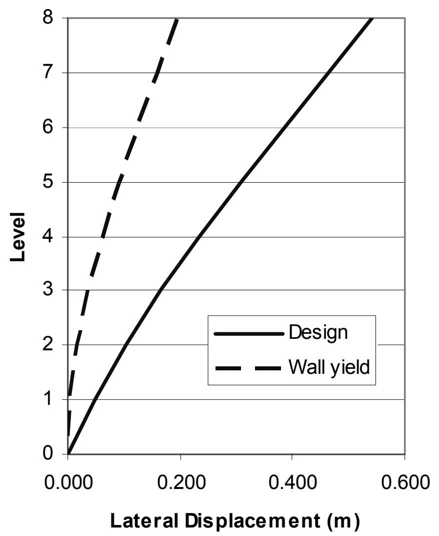

Figure 7: Displacement profiles for building at wall yield and at design deformation level.

Knowledge of the design displacement profile then enables most of the equivalent SDOF system properties to be established. The equivalent SDOF design displacement, Δ_d, effective mass, m_e, and effective height, h_e, for the case study building can be found using Equations 8 to 10 respectively.

$$\Delta_d = \frac{\sum_{i=1}^{n}\left(m_i\Delta_i^2\right)}{\sum_{i=1}^{n}\left(m_i\Delta_i\right)} = \frac{923}{2450} = 0.377m \tag{8}$$

$$m_e = \frac{\sum_{i=1}^{n}\left(m_i\Delta_i\right)}{\Delta_d} = \frac{2450}{0.377} = 6508T \tag{9}$$

$$h_e = \frac{\sum_{i=1}^{n}\left(m_i\Delta_i h_i\right)}{\sum_{i=1}^{n}\left(m_i\Delta_i\right)} = \frac{57134}{2450} = 23.3m \tag{10}$$

The sums performed within Equations 8 to 10 were undertaken in excel developing Table 2. One of the benefits of the Direct DBD is that the whole seismic design of this building can be undertaken using simple computations without the development of a computer analysis model. The seismic masses indicated in Table 2 were evaluated using the self weight of the structure together with expected imposed loads. Note that even though the roof level is only accessible for maintenance purposes, the seismic mass was approximately equal to that of other floors because a brown roof was proposed in which habitat is provided for nesting birds through provision of a gravelly soil layer that puts additional weight at roof level.

Table 2: Intermediate design values.

Level	Mass m_i (tonnes)	Δ_i (m)	$m_i\,\Delta_i$	$m_i\,\Delta_i^2$	$m_i\,\Delta_i\,h_i$
8	1088	0.54	591	321	18904
7	1088	0.46	504	233	14109
6	1088	0.38	418	161	10039
5	1088	0.31	335	103	6703
4	1088	0.24	256	60	4092
3	1088	0.17	181	30	2175
2	1088	0.10	113	12	904
1	1088	0.05	52	3	209
0	0	0.00	0	0	0
			2450	923	57134

In order to be able to undertake DBD the only remaining unknown is the equivalent viscous damping of the system. The means of obtaining this value for the rather peculiar dual system examined here is presented next.

Equivalent Viscous Damping of the Dual System

An equivalent viscous damping coefficient is used in the Direct DBD process to account for the effect that energy dissipation has on the seismic response. For RC wall structures the appropriate damping value is set in proportion to the expected displacement ductility demand, μ, using Equation 11 from [1].

$$\xi_{wall} = 0.05 + 0.444\left(\frac{\mu - 1}{\mu\pi}\right) \tag{11}$$

The displacement ductility of the wall is obtained by dividing the design displacement, Δ_d, from Equation 8, by the wall yield displacement obtained by substituting $h_i = h_e$ into Equation 4. For the case study structure $\Delta_{y,wall} = 0.117$ m and therefore the ductility and equivalent viscous damping for the walls equal 3.2 and 14.7% respectively.

In addition to the energy dissipated by the cyclic response of the RC walls, the EBF frame and viscous dampers also contribute to the energy dissipation and therefore the effective system damping needs to be obtained considering these components. Before detailing how this has been achieved for the case study in hand, consider Figure 8, which illustrates how the non-linear hysteretic response of the walls (with shear V_{wall} at displacement Δ_d) can be broken down into an equivalent viscous damping component, with maximum force F_{dwall}, in parallel with an elastic spring possessing an effective stiffness K_{eff}.

As can be seen in Figure 8, viscous damping provides a force that is velocity dependent, varying according to Equation 12.

$$F = Cv \tag{12}$$

where F is the damping force, v is the velocity and C is a constant expressed in units of force divided by velocity. As such, the viscous damping component is of an elliptical nature with a peak force at peak velocity (zero displacement) and zero force at the peak displacement, Δ_d. The peak damping force of the ellipse, F_d, can be shown to be given by Equation 13.

$$F_d = C\frac{2\pi\Delta_d}{T} \tag{13}$$

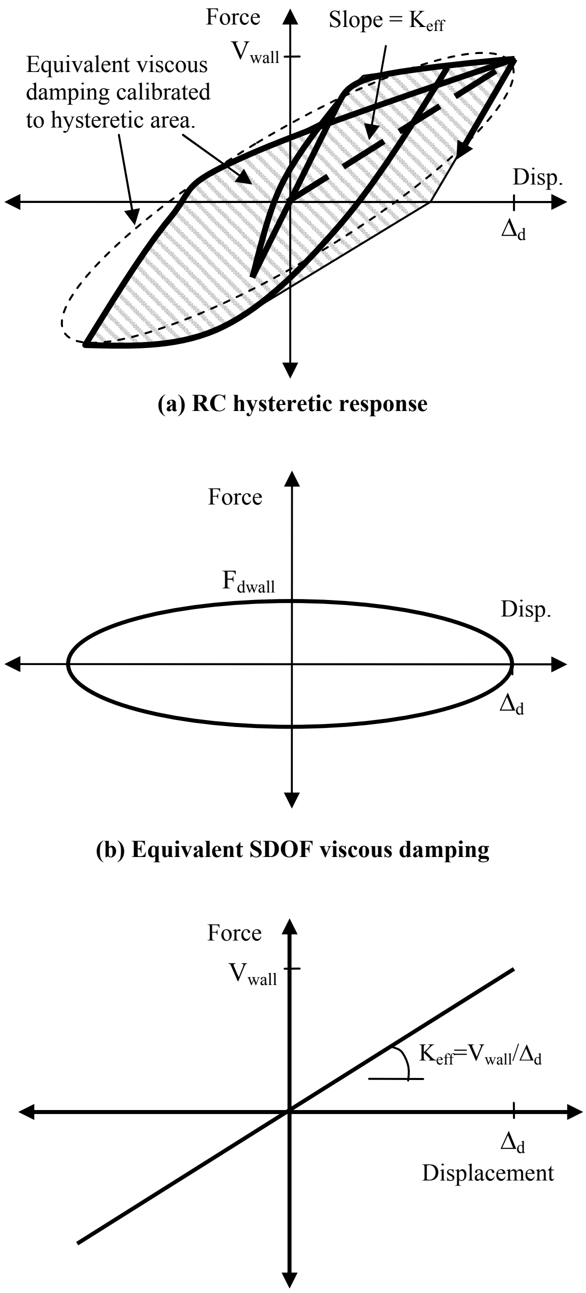

(a) RC hysteretic response

(b) Equivalent SDOF viscous damping

(c) Equivalent SDOF Effective Stiffness for RC walls

Figure 8: ***Equivalent SDOF viscous damping and effective stiffness components for RC walls (i.e. Non-linear dynamic response shown in (a) is approximated as the sum of (b) and (c)).***

The damping constant, C, can be related to the damping coefficient, ξ, through Equation 14.

$$C = \xi C_c = \xi 2m\omega_n = \xi\frac{4m\pi}{T} \tag{14}$$

Substituting Equation 13 into 14, and noting that $T^2 = 4\pi^2 m/K$ where $K = V/\Delta_d$, the peak damping force can be related to the viscous damping coefficient in accordance with Equation 15.

$$F_d = 2V\xi \tag{15}$$

Equation 15 is particularly useful for the hybrid dual system being considered here, as the equivalent damping forces for the separate elements of the system can be identified and summed to provide a total equivalent viscous damping force. This total damping force (provided by the dampers active in the direction of earthquake excitation being considered) can then be transformed into a system equivalent viscous damping ratio as shown in Equation 16.

$$\xi_{sys} = \frac{\sum F_d}{2V_b} \tag{16}$$

For the case study dual system, it has already been shown that the equivalent viscous damping coefficient for the RC walls is 14.7% (using Equation 11). It is also commonly assumed that elastic damping in steel structures is 2% and while this component could be considered negligible here, it is included for the EBF for illustrative purposes. Although the visco-elastic damper characteristics have not been decided yet, it was stated at the start of the design that the damper force would be set to provide three times the elastic force carried by the frame (i.e. $F_{damper} = 3*V_{EBF}$). Furthermore, it was stated that the EBF would resist 15% of the overturning at the design displacement, implying that the RC walls resist the remaining 85%. Consequently, using Equation 16, the strength proportions assigned at the start of the design procedure can be utilised to establish the system damping, as illustrated below.

$$\begin{aligned}\xi_{sys} &= \frac{2V_{wall}\xi_{wall} + 2V_{EBF}\xi_{EBF} + F_{damper}}{2V_b}\\ &= \frac{2*0.85*14.7\% + 2*0.15*2.0\% + 3*0.15}{2*1.00}\\ &= 35.3\%\end{aligned}$$

With the equivalent viscous damping for the dual system established, all the equivalent SDOF system parameters are now known and the standard Direct DBD procedure shown in Figure 3 can be followed to obtain the required member strengths.

Design Base Shear and Member Strengths

With the substitute structure characteristics (displacement, mass, height and damping) known, the required design strength of the system is obtained by identifying the value of effective period that will ensure the design displacement is not exceeded. This is done in line with Figure 3(d).

Firstly, the displacement spectrum needs to be scaled to the system damping level. This is achieved by using a damping-dependent scaling factor appropriate for the seismological characteristics of the design region. The Eurocode 8 [11] recommends that the η value obtained from Equation 17 be used to scale the elastic displacement spectrum to the damping level of interest.

$$\eta = \sqrt{10/(5+\xi_{sys})} \geq 0.55 \qquad (17)$$

As the case study structure being examined has been given very high damping properties, the scaling factor obtained from the left side of Equation 17 is 0.50. This value is less than the minimum limit of 0.55. However, it will be shown that the real records selected to undertake advanced verification analyses of the structural design in this work are fairly well predicted by Equation 17 even at higher levels of damping. As such, the value of 0.50 obtained from the left side of Equation 17 was used to scale demands and obtain the required effective period, T_e= 5.4s, as shown in Figure 9.

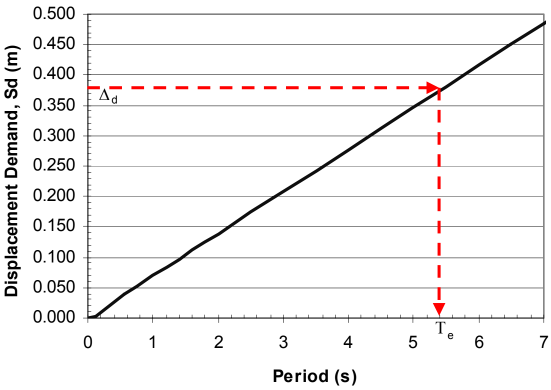

Figure 9: Determination of required effective period (displacement spectrum at 35.3% damping).

With the effective period known, the required effective stiffness, K_{eff}, is then obtained as per Equation 18.

$$K_{eff} = 4\pi^2 \frac{m_e}{T_e^2} = 4\pi^2 \frac{6508}{5.4^2} = 8702kN/m \qquad (18)$$

The total design base shear, V_b, is then found by multiplying the effective stiffness by the design displacement, as illustrated in Equation 19.

$$V_b = \Delta_d K_{eff} = 0.377 * 8702 = 3276kN \qquad (19)$$

And the design overturning moment is given by Equation 20.

$$M_{total} = V_b h_e = 3276 * 23.3 = 76400kNm \qquad (20)$$

Note that both the design base shear and overturning moment reported in Equations 19 and 20 are for half the building as the masses reported in Table 2 are for half the building and by symmetry the same design strengths will be required for the other half.

Maintaining the strength proportions set at the start of the design process, the required flexural strength (at the design deformation limit) of the 6 m U-shaped RC wall is then calculated as 85% of 76,400 kNm = 65,000 kNm. This value of overturning could conservatively be used to determine the required reinforcement in the wall. However, allowing for strain-hardening with a moment-curvature post yield stiffness ratio r_{curv}= 0.01, the required nominal strength of the wall is more accurately given by Equation 21.

$$M_{n,wall} = \frac{M^*}{1+r(\mu-1)} \qquad (21)$$
$$= \frac{65000}{1+0.01(10.2-1)} = 59500kNm$$

where the displacement ductility demand has been converted to a curvature ductility demand of 10.2 for use with r_{curv}.

Design of the EBF members needs to consider forces at both maximum displacement and maximum velocity (zero displacement). At maximum displacement it was stipulated that the EBF would resist 15% of the overturning. It was additionally decided that the damping force would be three times this value. Considering the geometry of the EBF shown in Figure 2, the link beam shear, V_{link}, can be obtained simply as the EBF overturning demand divided by the EBF length, as shown in Equation 22. The design values of link beam shear at peak displacement and peak velocity follow, as shown.

$$V_{link} = \frac{M_{EBF}}{L_{EBF}} \qquad (22)$$
$$= \frac{15\% * 76400}{18.3} = 626kN \quad \text{at max. displacement}$$
$$= 3 * \frac{15\% * 76400}{18.3} = 1880kN \quad \text{at max. velocity}$$

The design moments at the ends of the link beams are then obtained simply as the product of the link beam shear by the link beam span/2. As such, the maximum design moment to be resisted by the link beams is M* =1880*4/2 =3,760 kNm and the moment at peak displacement is equal 1,250 kNm. The bending moment diagram for the EBF at peak displacement response is shown in Figure 10.

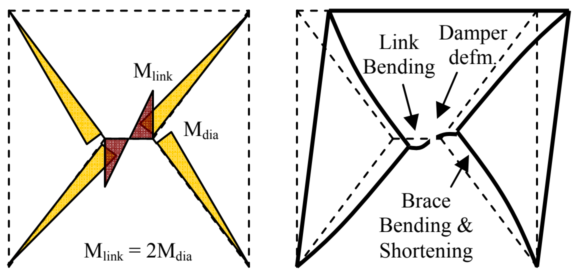

Figure 10: Bending moment diagram and deformed shape of EBF at design displacement.

Axial forces in the braces are obtained from equilibrium using the angle of the braces (66°) to be N_{dia}= 1,029 kN and 343 kN at the peak velocity and displacement respectively. 750 x 500 x 40 RHS and 500 x 40 mm SHS steel sections were selected to form the EBF link beams and diagonals respectively. It can be shown that these sections provide sufficient strength for the expected loads (which need to be factored to allow for capacity design requirements). Of particular interest here, however, are the deformations that would be expected of the EBF framing as this will affect the displacements imposed on the visco-elastic dampers. If the EBF were to rotate as a rigid-body either side of the damper, the vertical deformation imposed on the damper would be given by Equation 23.

$$\Delta_{Link,RigidEBF} = \frac{\Delta_r}{H} L_{EBF} = \frac{0.54}{32.0} * 18.3 = 0.310m \qquad (23)$$

where Δ_r is the displacement of the roof at the development of the design displacement, H is the total building height and L_{EBF} is the length of the EBF.

However, the actual deformation on the damper is less than this due to the effects of link-beam bending & shear deformations, bending and axial deformations in the diagonal braces, and even axial deformations in the main columns. For the 500x40 mm SHS section these deformation components were estimated (using simple moment-area theory & axial stiffness equations) to reduce the vertical deformation demand on the damper from 310 mm (as per Equation 21) to 277 mm. Note that the main deformation component in the EBF system is associated with bending of the diagonal braces. Rather than use hand calculations to undertake the deformation estimate, one could also apply the design lateral force to a simple structural model of the EBF system to consider the likely member deformations at peak response, but this is not absolutely necessary.

Knowing the peak displacement demand imposed on the damper, Δ_{damp}, the damping constant, C, required to provide the design damping force, F_{damper}, is computed as per Equation 24.

$$C = \frac{F_{damper} T_e}{\Delta_{damp} 2\pi} = \frac{1880 * 5.4}{0.277 * 2\pi} = 5870 kNs/m \quad (24)$$

The effective period of the building, T_e, is used in Equation 24 because the rigid-diaphragm action ensures that the walls and EBFs move together with the same effective period.

The stiffness required of the visco-elastic damper is obtained considering the force required at the peak displacement, as shown by Equation 25.

$$K_{damper} = \frac{F_{damper,\Delta\max}}{\Delta_{damper}} = \frac{626}{0.277} = 2261 kN/m \quad (25)$$

The damping constant and stiffness values provided by Equations 24 and 25 can then be provided to a damper manufacturer for the visco-elastic damper design. Note that while visco-elastic dampers are envisaged here, viscous dampers in parallel to elastic elements could also be utilised without changing the design procedure.

At this point the displacement-based design is complete as the required strength of the RC walls has been established, the EBF section sizes have been set, and the required visco-elastic damper characteristics have been established. Note that the whole design was possible without the need for complex analyses or the construction of a computer model. The next step in the seismic design would be to undertake capacity design of the elements not intended to yield. Details of capacity design are not reported here but it is noted that the maximum forces in the EBF are associated with the damper response and given uncertainties that exist in the demand velocity, a simplified capacity design approach when using linear viscous dampers is to assume that twice the velocity demand could develop [4].

DESIGN VERIFICATION UTILISING NON-LINEAR TIME-HISTORY ANALYSES

Eurocode 8 [11] does not yet include Direct DBD as an acceptable seismic design method. However, non-linear time-history analyses are permitted as a valid analysis method. Clearly, in a design office the use of non-linear time-history analyses is not practical early on at concept and scheme design phases owing to the considerable effort required to adequately model and analyse a structure. Furthermore, non-linear time-history analysis does not offer engineers a design tool as they are left to their own devices to set member strengths correctly.

The opportunity therefore exists for designers to use Direct DBD in practice for the quick development of various concept and scheme design solutions, with non-linear time-history analysis used to provide a code-compliant verification at the detailed design stage.

To investigate the performance of the concept design solution presented in this paper, non-linear time-history analyses have been carried out using Ruaumoko [12]. The five accelerograms listed in Table 3 were selected and the magnitude of the accelerations scaled to be spectrum compatible with the design displacement spectrum. The spectra of the scaled records are compared with the design spectrum for 5% damping in Figure 11.

Table 3: Accelerograms selected for NLTHAs.

Ref.	Earthquake Name	EQ Magnitude	Scale Factor
RR1	Imp. Valley, El Centro S90W	7.1	1.6
RR2	Loma Prieta, Hollister	7.1	1.9
RR3	Chi Chi, TCU010 N	7.6	2.2
RR4	Tabas, Boshrooy	7.7	3.6
RR5	Landers, Yermo	7.3	1.4

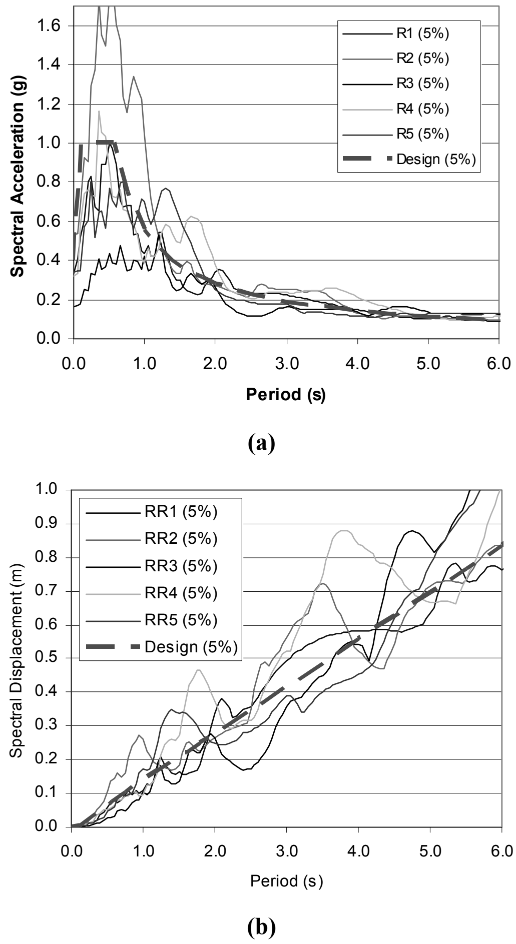

Figure 11: ***Comparison of (a) acceleration spectra and (b) displacement spectra at 5% damping for the selected accelerograms.***

An initial review of Figure 11 indicates that there is a large scatter in the spectra of the accelerograms and this will inevitably throw uncertainty on the evaluation of the methodology. However, as damping increases the spectra become more uniform. Furthermore, when the average of the spectral demands is compared with the design acceleration spectrum, the comparison is good, as shown in Figure 12(a). Moreover, as can be seen in Figure 12(b), the average of the displacement spectra at different levels of damping compare well with the design spectrum and indicate that the use of the EC8 damping modifier (Equation 17) was justified. This indicates that the accelerograms should impose similar levels of demand to those assumed in the design and thereby provide a reasonable evaluation of the performance of the methodology.

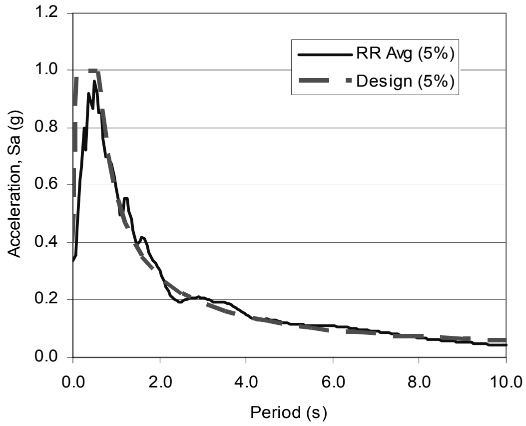

(a)

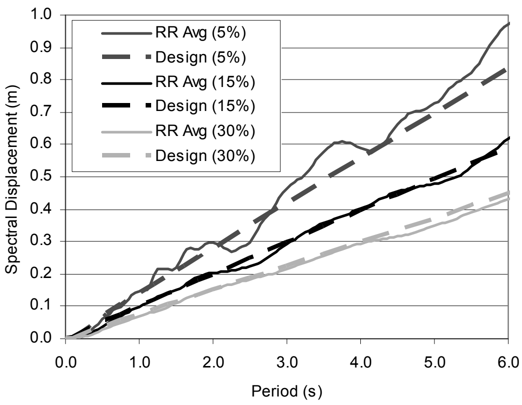

(b)

Figure 12: ***Comparison of (a) 5% damped average acceleration spectrum and (b) average of displacement spectra at 5%, 15% and 30% damping.***

Modelling Approach

A simple 2D model of the structure was developed in Ruaumoko [12], with the storey masses lumped at the wall centreline. The nodes of the walls and steel columns were constrained to move together, assuming that the floors behaved as rigid-diaphragms in-plane, infinitely flexible out-of-plane. Note however, that the diagonals of the EBF frame only connect to the building at the roof and ground levels, and therefore the EBF diagonal and link beam nodes were not constrained. The model developed in Ruaumoko is illustrated in Figure 13.

The RC walls and steel framing were modelled with Giberson beam elements (see Ruaumoko user manual [12]). Elastic properties were assigned to elements that are not intended to yield on the basis that appropriate capacity design would have ensured that inelasticity is concentrated only in regions associated with the intended plastic mechanism.

Two nodes were located at the centre of the link beam to enable the modelling of the visco-elastic dampers. The nodes were connected via a spring element, to model the elastic stiffness of the visco-elastic dampers, and a damper element to model the viscous damping properties. Stiffness and damping values obtained from the design process (Equations 24 and 25) were specified in the global vertical axis direction only.

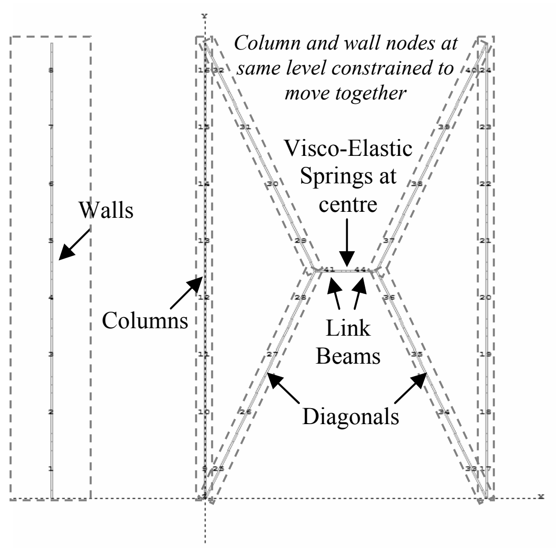

Figure 13: ***Plot of 2D structural model developed in Ruaumoko [12]. Element numbering from Ruaumoko is shown and different structural elements are indicted.***

The RC wall base hinge was provided a bending strength to exactly match the nominal strength obtained from the displacement-based design (Equation 21). The concrete hinges were characterised using the Takeda [13] hysteretic model, with 1% post-yield moment-curvature stiffness and the unloading model of Emori and Schonbrich [14]. Parameters for the Emori and Schonbrich model included an unloading stiffness factor of 0.5 together with a reloading stiffness factor of 0.0 and a reloading power factor of 1.0. Refer to the Ruaumoko manual [12] for further details. The plastic hinge length of the wall was calculated in line with the recommendations from Priestley *et al.* [1]. Small displacement analyses were undertaken and an integration time step of 0.001s was adopted.

There presently appear to be significant uncertainties in seismic engineering as to the appropriate amount of elastic damping that can be relied upon, and the best means of modelling this, particularly when higher modes are considered. For a discussion on the subject refer to [1]. For this case study the RC walls were assumed to respond with 5% elastic damping, whereas the steel frame was assumed to be characterised by 2% elastic damping. In order to try and reproduce this in the non-linear time-history analyses, the Rayleigh tangent stiffness damping model was adopted. Firstly, the 1st mode damping value that would provide the effect of 5% tangent stiffness damping for the RC wall system was found to be 2.2% in line with the recommendations of Priestley and Grant [15]. However, the walls respond in parallel with the steel frames which, as mentioned above, should be characterised with 2% elastic damping. Considering this, the relative work done by the steel frames and RC walls was used to factor the damping ratios and arrive at a 1st mode damping coefficient for the analyses of 2.17%. The relative work-done was also used to factor the damping value for the 2nd mode, which was subsequently set as 4.6%.

For the verification of the DBD method developed here, the effects of the damping model due to the uncertainties mentioned above are not expected to be very significant because the visco-elastic dampers have lead to very high system damping values. However, as will be discussed in reviewing the results, the dampers may not have been very active in resisting the higher mode response and therefore alternative damping models could affect the higher mode influence. Development of better means of quantifying and modelling elastic damping is an important area for future research.

Results of Non-linear Time-History Analyses

The maximum displacements recorded up the height of the structure for each of the earthquake records are shown in Figure 14. The maximum storey drifts, measured as the ratio of the relative storey displacement divided by the inter-storey height, are shown for each record in Figure 15. For both figures the values recorded are compared with the design target values.

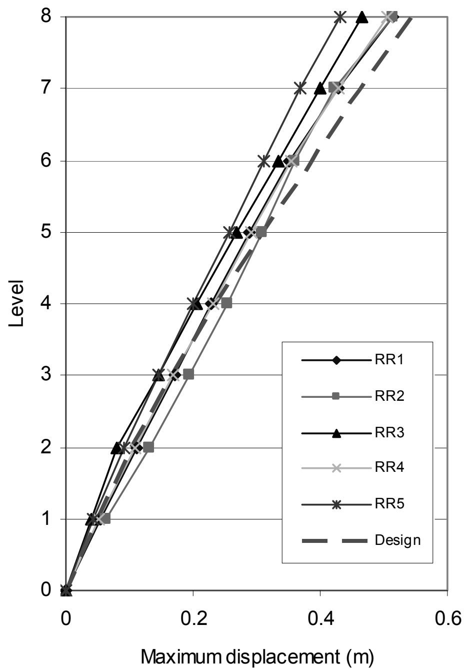

Figure 14: ***Maximum storey displacements recorded for the case study building.***

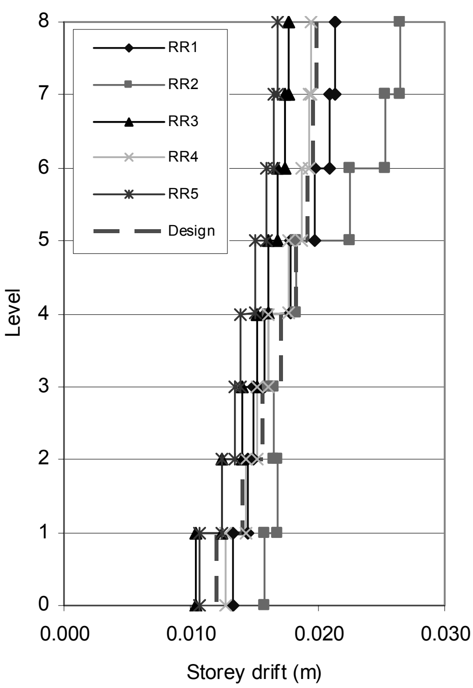

Figure 15: ***Maximum storey drifts recorded for the case study building.***

Reviewing the results presented in Figures 14 and 15, it is clear that the design deformation profile has been matched well. However, it is also evident that there is considerable scatter in the results, particularly for storey drifts. Record RR2 caused particularly large upper and lower storey drifts and this behaviour is attributed to the contribution of the second mode of vibration. To explain why, consider the displacement and storey drift profiles shown for different instances in time before and after the development of the peak storey drift (at 8.6s) for record RR2 in Figure 16 and 17 respectively.

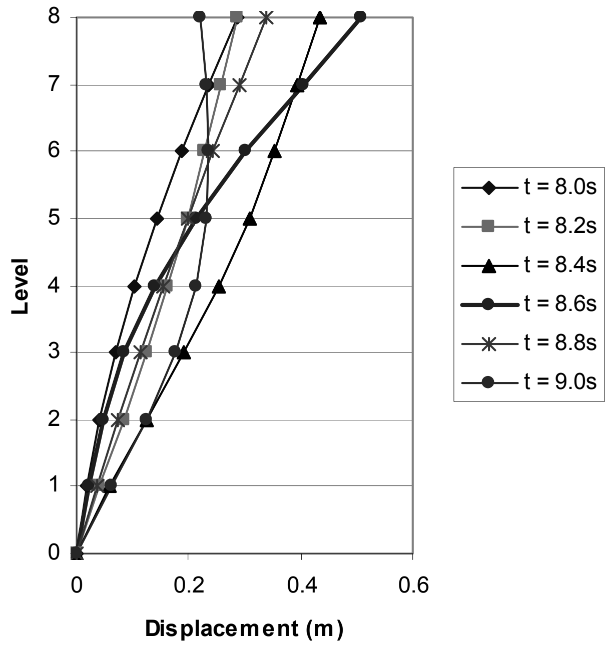

Figure 16: ***Displacement profiles at different instances in time before and after development of the peak storey drift for record RR2.***

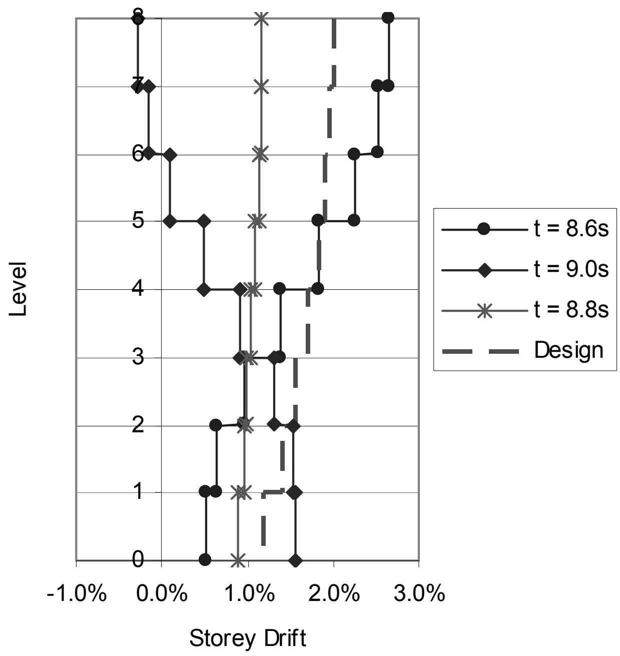

Figure 17: ***Storey drift profiles at different instances in time before and after development of the peak storey drift (at 8.6s) for record RR2.***

In reviewing Figures 16 and 17, one should recall that higher modes of vibration are characterised by significantly shorter periods of vibration than the fundamental mode. As such, if significant high frequency (small period) oscillations are observed in the dynamic response, these can be attributed to higher mode effects. While it is common to think of elastic higher modes of vibration, it should be apparent that higher mode effects are also to be expected when a structure is deforming inelastically. As a result, the characteristics of the higher modes present in the inelastic range will not be the same as elastic modes of vibration but are nevertheless present and can be very significant, as has been reported by many previous researchers of wall, frame and frame-wall structures such as Kabeyasawa [16], Eibl & Keintzel [17], Priestley and Amaris [18], Pettinga and Priestley [19] and Sullivan *et al.* [20].

For the case study structure being examined, the displacement profiles at 8.6s and 9.0s are characteristic of a 2nd mode of vibration in which upper levels are excited in an opposite direction to lower levels. This is also apparent from the quick changes in storey drifts that are presented in Figure 17. At 8.60s the displacement profile indicates that the 2nd mode is acting to significantly increase displacements and drifts over the upper storeys, at 8.80s the displacement profile appear to be fairly unaffected by the 2nd mode and the drift profile matches that assumed in design, whereas at 9.0s the 2nd mode appears to now be significantly reducing the displacements over the upper storeys. Based on the time elapsed between these response points, one could estimate the higher mode period of vibration as 0.8s (= 2.(9.0 - 8.6)). Note that this is a simplified assessment of higher modes, made for discussion purposes only and if more accurate values were required then signal analysis should be adopted, as was done for Frame-Wall structures by Sullivan *et al.* [20].

The large second mode oscillations recorded for record RR2 can be partly attributed to the particularly high spectral accelerations and displacement demands that record RR2 imposes at short periods, as evident in Figure 11. In addition however, as the EBF system provides a large restraint against movements only at roof level, higher modes may not have been as effectively reduced by the EBF visco-elastic dampers as the fundamental mode. If the positioning of a damper is such that during the oscillation of a particular mode of vibration the device is not deformed, the damper would not be expected to be effective in reducing the response of that particular mode of vibration. For the case study structure examined, the dampers in the EBF are only deformed if the roof displaces relative to the ground. Reviewing the difference in displaced shape at 8.4s and 8.6s shown in Figure 16, one observes that the roof displacements only increase by around 15% whereas the displacements of intermediate floors reduce by up to 50%. This might therefore suggest that the EBF dampers will have been less effective in restraining the vibration. However, additional research would be required to properly evaluate the effectiveness of the dampers on the higher mode response.

The apparent higher mode effects that have been observed suggest that the design procedure would be improved if an allowance for higher modes was made. However, the results presented in Figures 14 and 15 provide a good indication that the design methodology has performed well. Higher modes may have acted to cause significant scatter in the results, but when one considers the excellent correlation between the average of the maximum recorded displacements and storey drifts compared with the design values, in Figures 18 and 19 respectively, it is clear that the DBD approach offers a very powerful design tool.

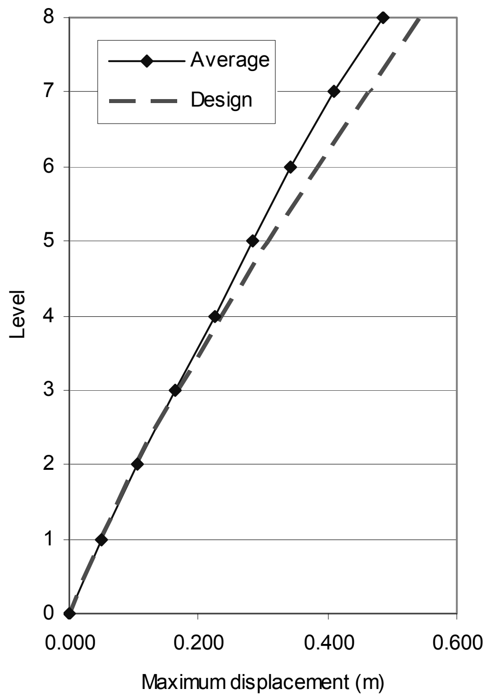

Figure 18: ***Average of maximum recorded storey displacements compared with the design displacement profile.***

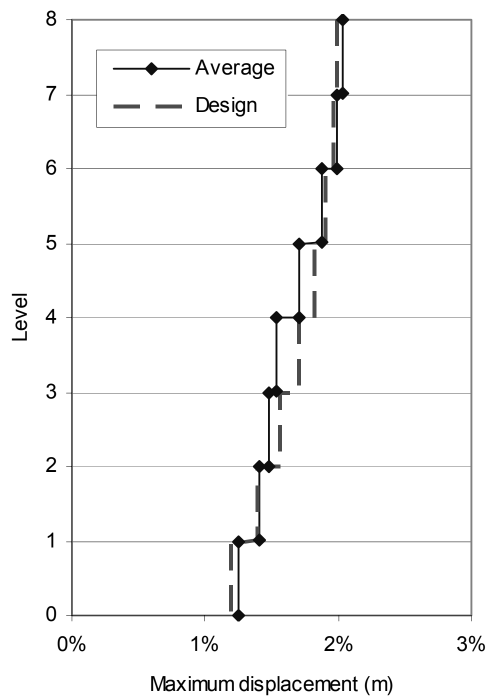

Figure 19: ***Average of maximum recorded storey drifts compared with the design drift profile.***

CONCLUSIONS

An innovative application of Direct DBD has been presented for a modern 8-storey dual system structure consisting of interior concrete walls in parallel to a number of large steel eccentrically braced frames, linked with visco-elastic dampers. The methodology developed permits the designer to directly control the forces developed in the structure by choosing strength proportions at the start of the design procedure. These strength proportions are used to establish the likely displaced shape at peak response and thereby characterise the equivalent single-degree-of-freedom system. In addition, a novel means of quickly establishing the equivalent viscous damping for a system with added dampers has been presented which utilises the strength proportions assigned by the designer. The DBD approach developed is relatively quick, enabling the seismic design of the 8-storey case study structure to be undertaken without the development of a computer model. Non-linear time-history analyses have been used to demonstrate that the design solution successfully achieves the design objectives to limit building deformations, and therefore damage. The work provides a clear example as to how designers can and should start to take advantage of displacement-based design in practice.

REFERENCES

1. Priestley, M.J.N., Calvi, G.M. & Kowalsky, M. J. (2007) "Direct Displacement-Based Seismic Design". *IUSS Press*, www.iusspress.it, Pavia, Italy. 720 pages.

2. ICBO, (1997) "Uniform Building Code". *International Conference of Building Officials*, Whittier, California, USA.

3. Sullivan, T.J., Priestley, M.J.N., Calvi, G.M. (2006) "Seismic Design of Frame-Wall Structures". *Research Report ROSE-2006/02*, *IUSS press*: www.iusspress.it, 303 pages.

4. Christopolous, C., Filiatrault, A. (2007) "Principles of Passive Supplemental Damping and Seismic Isolation" *IUSS Press*, Pavia, Italy. (www.iusspress.it).

5. Gulkan, P., Sozen, M. (1974) "Inelastic response of reinforced concrete structures to earthquake motions." *ACI Journal*, **71** (12), pp.604-610.

6. Shibata, A., Sozen, M.A. (1976) "Substitute Structure Method for Seismic Design in Reinforced Concrete" *Journal of the Structural Division, ASCE*, **102** (ST1).

7. Sullivan, T.J., Priestley, M.J.N., Calvi, G.M., (2004) "Displacement shapes of frame-wall structures for direct displacement based design" *Proceedings of Japan-Europe 5th workshop on implications of recent earthquakes on seismic risk*, Bristol.

8. Beyer, K., Dazio, A., Priestley, M.J.N., (2008) "Seismic Design of Torsionally Eccentric Buildings with RC U-shaped walls" *Research Report ROSE-2008/03*, IUSS press: www.iusspress.it.

9. Paulay, T. (2003). "Seismic displacement capacity of ductile reinforced concrete building systems". *Bulletin of New Zealand Society for Earthquake Engineering*, **36**(1).

10. Priestley, M.J.N., Paulay, T. [2002] "What is the stiffness of reinforced concrete walls". *SESOC Journal*, Structural Engineering Society of New Zealand, Vol. **15**, No.1, pp.30-34.

11. CEN (1998) "Eurocode EC8 - Design of structures for earthquake resistance - Part 1: General rules, seismic actions and rules for buildings, prEN-1998-1," *Comite Europeen de Normalization*, Brussels, Belgium.

12. Carr, A.J. (2004) *Ruaumoko3D – A program for Inelastic Time-History Analysis*, Department of Civil Engineering, University of Canterbury, New Zealand.

13. Otani, S. (1981) "Hysteresis models of reinforced concrete for earthquake response analysis". *Journal of the Faculty of Engineering*, University of Tokyo, Vol. **XXXVI**, No.2, pp125-159.

14. Emori, K., and Schonbrich, W.C. (1978) "Analysis of Reinforced Concrete Frame-Wall Structures for Strong Motion Earthquakes". Civil Engineering Studies, Structural Research Series No. 434, *University of Illinois*, Urbana. Illinois, USA.

15. Priestley, M.J.N., Grant, D.N. (2006) "Viscous damping for analysis and design". *Journal of Earthquake Engineering*, **9**(SP2), pp229-255.

16. Kabeyasawa, T., (1987) "Ultimate-state design of reinforced concrete wall-frame structures". *Proceedings of Pacific Conference on Earthquake Engineering*, Wairakei, New Zealand, Vol. **1**.

17. Eible, J., Keintzel, E., (1988) "Seismic Shear Forces in Reinforced Cantilever Shear Walls". *Proceedings of the 9th World Conference on Earthquake Engineering*, Paper 1-1, Tokyo- Kyoto, Japan.

18. Priestley, M.J.N. and Amaris, A., (2002) "Dynamic Amplification of Seismic Moments and Shear Forces in Cantilever Walls". Report No. ROSE 2002/01, *IUSS Press:* www.iusspress.it, 86 pages.

19. Pettinga, J.D. and Priestley, M.J.N., (2005) "Dynamic Behaviour of Reinforced Concrete Frames Designed with Direct Displacement-Based Design". Report No. ROSE 2005/02, *IUSS press*: www.iusspress.it, 154 pages.

20. Sullivan, T.J., Priestley, M.J.N. and Calvi, G.M., (2008) "Estimating the Higher Mode Response of Ductile Structures". *Journal of Earthquake Engineering,* Vol.**12**, No. 3, pp456–472.